Title	The hyperfine structure of the 13 g state of Na 2
Author(s)	Liu, Y; Ji, B; Cheung, ASC; Stwalley, WC; Field, RW; Lyyra, AM; Li, L
Citation	Journal Of Chemical Physics, 2001, v. 115 n. 8, p. 3647-3656
Issued Date	2001
URL	http://hdl.handle.net/10722/42038
Rights	Journal of Chemical Physics. Copyright © American Institute of Physics.

The hyperfine structure of the 1 $^3\Delta_g$ state of Na$_2$

Y. Liu
Department of Physics and Key Lab of Atomic and Molecular Nanosciences, Tsinghua University, Beijing 100084, China

B. Ji
Department of Physics, University of Connecticut, Storrs, Connecticut 06269-3046

A. S.-C. Cheung
Department of Chemistry, The University of Hong Kong, Hong Kong

W. C. Stwalley
Department of Physics, University of Connecticut, Storrs, Connecticut 06269-3046

R. W. Field
Department of Physics and Key Lab of Atomic and Molecular Nanosciences, Tsinghua University, Beijing 100084, China and Department of Chemistry, Massachusetts Institute of Technology, Massachusetts 02139

A. M. Lyyra
Department of Physics, Temple University, Philadelphia, Pennsylvania 19122

Li Li[a)]
Department of Physics and Key Lab of Atomic and Molecular Nanosciences, Tsinghua University, Beijing 100084, China

The hyperfine spectra of the Na$_2$ 1 $^3\Delta_g$ state have been recorded with sub-Doppler continuous wave (CW) perturbation facilitated optical–optical double resonance (PFOODR) spectroscopy via $A\ ^1\Sigma_u^+ \sim b\ ^3\Pi_u$ mixed intermediate levels. The rotational lines into the $N=14$–51 levels of the 1 $^3\Delta_g$ state observed previously [J. Mol. Spectrosc. **134**, 50 (1989)] have four components for transitions between symmetric rotational levels or five components for transitions between antisymmetric rotational levels and the hyperfine coupling belongs to Hund's case $b_{\beta S}$. For the low-N levels observed later, however, the hyperfine spectra are much more complicated. We have worked out the matrix elements of the molecular Hamiltonian in the case $b_{\beta S}$ basis. After taking into consideration spin–orbit, spin–spin, and spin–rotation interactions, we obtained a set of molecular constants for the Na$_2$ 1 $^3\Delta_g$ state, with which we can reproduce the hyperfine spectra of both high- and low-N rotational levels. © *2001 American Institute of Physics.* [DOI: 10.1063/1.1388548]

I. INTRODUCTION

There are many theoretical and experimental studies of hyperfine structure (HFS) in molecular spectroscopy.[1–9] Alkali metal diatomic molecules have received much attention in hyperfine research.[10–21] The sodium dimer, one of the most important alkali metal dimers, is an exemplary molecule for studying hyperfine spectroscopy, due to the nonzero nuclear spin, $I_1=I_2=3/2$, of Na atoms. The total nuclear spin quantum number $I=I_1+I_2$ can be 3, 2, 1, 0. The nuclear spin wave function of Na$_2$ is symmetric for $I=3$, 1, or antisymmetric for $I=2$, 0.

The hyperfine splitting of the Na$_2$ 1 $^3\Delta_g$ state has been resolved by sub-Doppler CW perturbation facilitated optical–optical double resonances (CW PFOODR) fluorescence excitation spectroscopy.[10] In Ref. 10, Li *et al.* analyzed the hyperfine splittings of transitions to high-N levels (N

$=14$–51, N is the rotational quantum number) of the 1 $^3\Delta_g$ state from intermediate $A\ ^1\Sigma_u^+ \sim b\ ^3\Pi_{1u}$ mixed levels. They successfully explained the hyperfine splittings with the Fermi contact interaction $b_F\mathbf{I}\cdot\mathbf{S}$[1] term. We report here the hyperfine structure of transitions to low-N levels of the Na$_2$ 1 $^3\Delta_g$ state. This structure turns out to be much more complicated than that of the high-N levels. Hyperfine patterns at high-N are only partially resolved according to their quantum number $G(\mathbf{G}=\mathbf{I}+\mathbf{S})$.[1,22] The $F(\mathbf{F}=\mathbf{G}+\mathbf{N})$ components of each G are not resolved. At low-N, the intervals between hyperfine splittings become larger and thus the low-N hyperfine spectra become much more complex and more completely resolved. Although the Fermi contact interaction term alone is sufficient to interpret high-N hyperfine spectra, it is not sufficient to explain the observed low-N hyperfine splittings. In order to satisfactorily explain the hyperfine spectra obtained for the entire range of N, we have derived the Hamiltonian matrix element in the case $b_{\beta S}$ coupling scheme, including spin–orbit, spin–rotation, spin–spin, and magnetic interactions.

[a)]Author to whom correspondence should be addressed. Electronic mail: lili@lsad.tsinghua.edu.cn

Using such an effective hyperfine Hamiltonian, we have successfully explained the hyperfine structure of these spectra and obtained a set of molecular constants for the $1\,^3\Delta_g$ state of Na$_2$.

II. OBSERVATION

Sub-Doppler CW PFOODR spectroscopy has been used to observe the hyperfine structure of the Na$_2$ $1\,^3\Delta_g$ state. The experimental setup has been reported elsewhere.[23] Briefly, a five-arm heatpipe oven was used to generate sodium vapor. The sodium vapor temperature was around 500 °C with ~0.5 Torr argon as buffer gas. Two CR899-29 ring dye lasers were used as the PUMP and PROBE lasers. The two laser beams were co-propagated along the axis of the heatpipe. The PUMP laser frequency was held fixed to excite an $A\,^1\Sigma_u^+$ $\sim b\,^3\Pi_{1u} \leftarrow X\,^1\Sigma_g^+$ transition and the PROBE laser frequency was scanned to further excite the molecule from the intermediate state to the $1\,^3\Delta_g$ state. The OODR excitation signals were detected with an ion detector through the associative ionization (Na$_2^*$+Na→Na$_3^+$+e$^-$).[24]

The $A\,^1\Sigma_u^+$ $v=22 \sim b\,^3\Pi_u$ $v=25$ levels are mixed by spin–orbit interaction and have been studied by sub-Doppler laser-induced fluorescence spectroscopy in a molecular beam.[25] The rotational levels of the $b\,^3\Pi_{1u}$ component intersect the $A\,^1\Sigma_u^+$ $v=22$ levels at $J=4$. The term values and mixing coefficients of the $A\,^1\Sigma_u^+ v=22 \sim b\,^3\Pi_u v=25$, $J=0\text{–}10$ levels can be obtained by diagonalizing the $A\,^1\Sigma_u^+ \sim b\,^3\Pi_u$ interaction matrix. The hyperfine structure of the $b\,^3\Pi_u v=25$ levels has been studied.[11] All rotational levels with predominant $^3\Pi_1$ character have no resolvable HFS at 20 MHz resolution. In our sub-Doppler fluorescence excitation experiment, we used $b\,^3\Pi_{1u}$ levels as intermediate state *window* levels. Since both the ground state and the intermediate levels do not have resolvable HFS, the HFS splitting in our PFOODR excitation spectra is due exclusively to the upper $1\,^3\Delta_g$ state.[10]

III. THEORY

There are many publications on the theory of hyperfine structure of diatomic molecules.[1,26–30] The spin–orbit constant for the Na$_2$ $1\,^3\Delta_g$ state is very small, while the Fermi-contact interaction constant is relatively large.[10] The logical choice of angular momentum coupling case for the $1\,^3\Delta_g$ state is therefore Hund's case $b_{\beta S}$. Molecular coupling schemes including nuclear spin are shown in Ref. 31. We will express the matrix elements in the Hund's case $b_{\beta S}$ basis set. The effective Hamiltonian (within a given vibrational state) can be written as

$$\mathbf{H}=\mathbf{H}^{\text{rot}}+\mathbf{H}^{\text{so}}+\mathbf{H}^{\text{ss}}+\mathbf{H}^{\text{sr}}+\mathbf{H}^{\text{mag.hyp}}+\mathbf{H}^{\text{quadrupole}}, \quad (1)$$

where

$$\mathbf{H}^{\text{rot}}=B\mathbf{N}^2-D\mathbf{N}^4,$$

rotational and centrifugal distortion energy, (2)

$$\mathbf{H}^{\text{so}}=A\mathbf{L}\cdot\mathbf{S}, \quad \text{spin–orbit interaction,} \quad (3)$$

$$\mathbf{H}^{\text{ss}}=\tfrac{2}{3}\lambda(3\mathbf{S}_z^2-\mathbf{S}^2), \quad \text{spin–spin interaction,} \quad (4)$$

$$\mathbf{H}^{\text{sr}}=\gamma\mathbf{N}\cdot\mathbf{S}, \quad \text{spin–rotation interaction,} \quad (5)$$

$$\mathbf{H}^{\text{mag.hyp}}=\alpha\mathbf{I}\cdot\mathbf{L}+b_F\mathbf{I}\cdot\mathbf{S}+\tfrac{1}{3}c(3\mathbf{I}_z\mathbf{S}_z-\mathbf{I}\cdot\mathbf{S}),$$

magnetic hyperfine interaction, (6)

$$\mathbf{H}^{\text{quadrupole}}=-e\mathbf{T}^2(\mathbf{Q})\cdot\mathbf{T}^2(\nabla\mathbf{E}),$$

nuclear electric quadrupole interaction.[1]

(7)

Where e is the electronic charge, the incorporation of the minus sign to the Hamiltonian is to conform with the IUPAC recommendations.[32] Due to the Rydberg character of the electronic states, the effects of the nuclear electric quadrupole interaction is small, this Hamiltonian term has not been used in our analysis.

The parameters in the magnetic hyperfine Hamiltonian of Eq. (6) are[8,31,33]

$$a=g_S g_N \mu_B \mu_N \sum_i \left\langle \frac{1}{r_i^3} \right\rangle_{\text{av}}, \quad (8)$$

$$b_F=\frac{8\pi}{3} g_S g_N \mu_B \mu_N \sum_i \langle \psi_i^2(r_i=0) \rangle_{\text{av}}, \quad (9)$$

$$c=\frac{3}{2} g_S g_N \mu_B \mu_N \sum_i \left\langle \frac{3\cos^2\theta_i-1}{r_i^3} \right\rangle_{\text{av}}. \quad (10)$$

Here μ_B and μ_N are the Bohr and nuclear magnetons, $g_S(g_S=2.0023^{3,34})$ and g_N are the electron spin g-factor and nuclear spin g-factor, respectively, and $\mathbf{r}_i$, θ_i are the spherical polar coordinates of electron-i, defined with respect to the nucleus under consideration. The average is over the valence electrons. The term $a\mathbf{I}\cdot\mathbf{L}$ represents the nuclear spin-electronic orbital angular momentum interaction, $b_F\mathbf{I}\cdot\mathbf{S}$ represents the Fermi contact interaction,[33] and the c term represents the dipolar electronic spin–nuclear spin interaction.

The wave function for the $1\,^3\Delta_g$ state in the case $b_{\beta S}$ coupling basis set is symbolized by $|\Lambda N(SI)GF\rangle$.

The matrix element of the rotational term [Eq. (2)] is diagonal in the case $b_{\beta S}$ basis and is given as

$$\langle \Lambda N(SI)GF|\mathbf{H}^{\text{rot}}|\Lambda N(SI)GF\rangle$$
$$=BN(N+1)-D[N(N+1)]^2. \quad (11)$$

Matrix elements of Eqs. (3)–(7) can be expressed compactly using the spherical tensor formalism.[35,36]

The spin–orbit matrix elements are

$$\langle \Lambda N'(SI)G'F|\mathbf{H}^{SO}|\Lambda N(SI)GF\rangle$$

$$= A\Lambda(-1)^{N+G'+F}\begin{Bmatrix} F & N & G \\ 1 & G' & N' \end{Bmatrix}$$

$$\times (-1)^{I+S+G+1}\sqrt{(2G+1)(2G'+1)}$$

$$\times \begin{Bmatrix} I & G' & S \\ 1 & S & G \end{Bmatrix}\sqrt{S(S+1)(2S+1)}$$

$$\times (-1)^{N'-\Lambda}\sqrt{(2N+1)(2N'+1)}\begin{pmatrix} N' & 1 & N \\ -\Lambda & 0 & \Lambda \end{pmatrix}. \tag{12}$$

The spin–spin matrix elements are

$$\langle \Lambda N'(SI)G'F|\mathbf{H}^{SO}|\Lambda N(SI)GF\rangle$$

$$= \frac{2}{3}\lambda(-1)^{N+G'+F}\begin{Bmatrix} F & G & N \\ 2 & N' & G' \end{Bmatrix}$$

$$\times (-1)^{I+S+G+2}\sqrt{(2G+1)(2G'+1)}\begin{Bmatrix} I & G' & S \\ 2 & S & G \end{Bmatrix}$$

$$\times [S(S+1)(2S-1)(2S+1)(2S+3)]^{1/2}$$

$$\times (-1)^{N'-\Lambda}\sqrt{(2N+1)(2N'+1)}\begin{pmatrix} N' & 2 & N \\ -\Lambda & 0 & \Lambda \end{pmatrix}, \tag{13}$$

and the spin–rotation matrix elements are

$$\langle \Lambda N'(SI)G'F|\mathbf{H}^{sr}|\Lambda N(SI)GF\rangle = \delta_{NN'}\gamma(-1)^{N+G'+F}\begin{Bmatrix} F & G' & N \\ 1 & N & G \end{Bmatrix}\sqrt{N(N+1)(2N+1)}(-1)^{I+S+G+1}$$

$$\times \sqrt{(2G+1)(2G'+1)}\begin{Bmatrix} I & G' & S \\ 1 & S & G \end{Bmatrix}\sqrt{S(S+1)(2S+1)}. \tag{14}$$

Magnetic hyperfine matrix elements can be separated into three additive terms, nuclear spin–electron orbital interaction, Fermi-contact interaction, and the spin dipolar term. The Fermi-contact interaction matrix is exclusively diagonal in the case $b_{\beta S}$ basis

$$\langle \Lambda N(SI)GF|b_F\mathbf{I}\cdot\mathbf{S}|\Lambda N(SI)GF\rangle = \frac{b_F}{2}[G(G+1)-I(I+1)-S(S+1)]. \tag{15}$$

The nuclear spin–electron orbit interaction matrix elements are similar in form to the spin–orbit matrix elements

$$\langle \Lambda N'(SI)G'F|a\mathbf{I}\cdot\mathbf{L}|\Lambda N(SI)GF\rangle = a\Lambda(-1)^{N+G'+F}\begin{Bmatrix} F & G & N \\ 1 & N' & G' \end{Bmatrix}(-1)^{I+S+G'+1}\sqrt{(2G+1)(2G'+1)}$$

$$\times \begin{Bmatrix} S & G & I \\ 1 & I & G' \end{Bmatrix}\sqrt{I(I+1)(2I+1)}(-1)^{N'-\Lambda}\sqrt{(2N+1)(2N'+1)}\begin{pmatrix} N' & 1 & N \\ -\Lambda & 0 & \Lambda \end{pmatrix}, \tag{16}$$

and the dipolar interaction matrix elements are

$$\langle \Lambda N'(SI)G'F|cI_zS_z|\Lambda N(SI)GF\rangle = c\frac{\sqrt{30}}{3}(-1)^{N+G'+F}\begin{Bmatrix} F & G' & N' \\ 2 & N & G \end{Bmatrix}\sqrt{I(I+1)(2I+1)}\sqrt{S(S+1)(2S+1)}$$

$$\times \sqrt{(2G+1)(2G'+1)}\begin{Bmatrix} S & S & 1 \\ I & I & 1 \\ G' & G & 2 \end{Bmatrix}(-1)^{N'-\Lambda}\sqrt{(2N+1)(2N'+1)}\begin{pmatrix} N' & 2 & N \\ -\Lambda & 0 & \Lambda \end{pmatrix}, \tag{17}$$

From the above expressions of the matrix elements, Eqs. (11)–(17), and the properties of the 3-j, 6-j, and 9-j symbols,[36] $\Delta N = N - N'$ can be 0, ± 1, and ± 2, $\Delta G = G - G'$ can be 0, ± 1, and ± 2, and $\Delta I = 0, \pm 1$. When the nuclear spin quantum number I changes by one quantum, the symmetry of the nuclear wave function must change from symmetric (antisymmetric) to antisymmetric (symmetric). Thus the only allowed value for ΔI is 0. The full matrix has the following properties:

(a) real symmetric;
(b) diagonal in F;
(c) diagonal in I;
(d) off-diagonal in $G(\Delta G = 0; \pm 1; \pm 2)$ and $N(\Delta N = 0; \pm 1; \pm 2)$.

In order to obtain the hyperfine eigenenergies, we must first set up and then diagonalize the matrix. The dimensions of

the Hamiltonian matrix for different rotational quantum numbers N are listed below:

	Dimension of the Hamiltonian matrix	
N	Antisymmetric rotational levels ($I=3,1$)	Symmetric rotational levels ($I=2,0$)
2	82	52
3	112	70
4	142	88
5	148	90
≥ 6	150	90

IV. RESULTS AND DISCUSSION

The intermediate $b\ ^3\Pi_u \Omega=1$ levels have no resolvable hyperfine splittings at 20 MHz resolution.[11] Our sub-Doppler resolution was 50 MHz. Thus the hyperfine splittings measured in the PFOODR excitation lines are due solely to the $1\ ^3\Delta_g$ upper state.

A. Fermi contact interaction

The previously reported OODR excitation spectra of the Na$_2$ $1\ ^3\Delta_g$ $N=14-51$ rotational levels exhibit a five line pattern for transitions between antisymmetric rotational levels ($I=3,1$) and a four line pattern for transitions between symmetric rotational levels ($I=2,0$). No additional structure was resolved within any of the 5 (or 4) lines. These rotational levels are well described by the case $b_{\beta S}$ hyperfine coupling scheme and dominated by the Fermi-contact interaction, which describes the contribution from the s-electron density at the nucleus, $\psi^2(0)$. Li *et al.*[10] predicted that the Fermi contact constants of the Na$_2$ and Li$_2$ triplet Rydberg states will all be about 1/4 of the values of the Fermi contact constants of the ground-state atoms [$b_F(^7\text{Li}\ 2s^2 S)=402$ MHz, and $b_F(\text{Na}\ 3s^2 S)=886$ MHz]. The experimentally determined b_F value from the $N=14-51$ levels is 210 ± 8 MHz for the Na$_2$ $1\ ^3\Delta_g$ state. Hyperfine splittings of other triplet Rydberg states of Na$_2$ and Li$_2$ were also resolved and the Fermi-contact constants obtained experimentally were found to agree quite well with the predicted values.

Since the Fermi contact interaction is not N-dependent, we will use $b_F=220$ MHz as its initial value in our calculations and simulations.

B. Spin–orbit interaction

At the case $b_{\beta S}$ coupling limit, $\mathbf{S}$ and $\mathbf{I}$ couple to yield $\mathbf{G}$ and $\mathbf{G}$ then couples with $\mathbf{N}$ to produce $\mathbf{F}$. For the $1\ ^3\Delta_g$ $N=14-51$ levels, the hypermultiplets are well described by $E_{N,G,I}=(b_F/2)[G(G+1)-S(S+1)-I(I+1)]$, and the F splittings within each G component were unresolved for all $N=14-51$ levels at 50 MHz resolution.

At high-N the angular momentum coupling scheme for the Na$_2$ $1\ ^3\Delta_g$ state is close to Hund's case b[37] due to weak spin–orbit interaction. However, at low N, the spin–orbit interaction will have an important effect on the hyperfine structure. The HFS of the Na$_2$ $4\ ^3\Sigma_g^+$ state has been studied by PDOODR fluorescence excitation spectroscopy and the

coupling scheme is case $b_{\beta S}$ with $b_F=214\pm 50$ MHz. Since this is a $^3\Sigma$ state and its spin–orbit splitting is zero, the low-N HFS pattern remains case $b_{\beta S}$.

The $1\ ^3\Delta_g$ state is a $3d\delta$ Rydberg state[38] and asymptotically dissociates to the $3s+3d$ atomic limit. The electronic configuration of the $1\ ^3\Delta_g$ state is predominantly $(\sigma_g 3s)(3d\delta_g)$. The spin–orbit interaction arises mainly from the spin–orbit interaction of the Na atom $3d$ state, as in the case of the NaK $1\ ^3\Delta$ state.[39] The spin–orbit splitting between the $3d(^2D_{5/2})$ and $3d(^2D_{3/2})$ components is very small, $E(^2D_{5/2})-E(^2D_{3/2})=1.48$ GHz.[40] In Ref. 41 a simple relation between the atomic spin–orbit constant and molecular spin–orbit splittings was derived semiempirically. For the Na $3d(^2D_{5/2})$ state, the wave function is $|\delta\alpha\rangle$, and for the $3d(^2D_{3/2})$ state the wave function is $|\delta\beta\rangle$, where δ symbolizes the $m_l=2$ projection for the $l=2$ atomic angular momentum on the internuclear axis, and α and β symbolize electronic spin projection quantum numbers $m_s=+1/2$ and $-1/2$, respectively. The spin–orbit interaction Hamiltonian for the Na $3d$ state is

$$\mathbf{H}^{\text{so}}=a\mathbf{l}\cdot\mathbf{s}. \tag{18}$$

The eigenenergy for the $^2D_{5/2}$ state is

$$
\begin{aligned}
E_{5/2} &= \langle ^2D_{5/2}|\mathbf{H}^{\text{so}}|^2D_{5/2}\rangle \\
&= \langle ^2D_{5/2}|a\mathbf{l}\cdot\mathbf{s}|^2D_{5/2}\rangle \\
&= \langle \delta\alpha|a\mathbf{l}\cdot\mathbf{s}|\delta\alpha\rangle \\
&= 2\times\tfrac{1}{2}\times\langle 3d|a|3d\rangle \\
&= a_{3d}.
\end{aligned} \tag{19}
$$

From the angular momentum relation $\mathbf{j}=\mathbf{l}+\mathbf{s}$, $\mathbf{l}\cdot\mathbf{s}=\tfrac{1}{2}(\mathbf{j}^2-\mathbf{l}^2-\mathbf{s}^2)$, the eigenenergy for Na $3d\,^2D_{5/2}$ can be expressed in another form

$$
\begin{aligned}
E_{5/2} &= \langle ^2D_{5/2}|\mathbf{H}^{\text{so}}|^2D_{5/2}\rangle \\
&= \langle ^2D_{5/2}|a\mathbf{l}\cdot\mathbf{s}|^2D_{5/2}\rangle \\
&= \tfrac{1}{2}[j(j+1)-l(l+1)-s(s+1)]\zeta \\
&= \zeta,
\end{aligned} \tag{20}
$$

where

$$\zeta = \left\langle 3d\left|\frac{\alpha^2}{2}\frac{Z_{\text{eff}}}{r^3}\right|3d\right\rangle^{41}, \tag{21}$$

and $\mathbf{j}=\mathbf{l}+\mathbf{s}$ (here $l=2$, $s=1/2$ for $^2D_{5/2}$, and $j=5/2$).

From Eqs. (19) and (20)

$$a_{3d}=\zeta. \tag{22}$$

The eigenenergy for $3d(^2D_{3/2})$ is

$$
\begin{aligned}
E_{3/2} &= \langle ^2D_{3/2}|\mathbf{H}^{\text{so}}|^2D_{3/2}\rangle \\
&= \tfrac{1}{2}[j(j+1)-s(s+1)-l(l+1)]\zeta \\
&= -\tfrac{3}{2}\zeta.
\end{aligned} \tag{23}
$$

From Eqs. (20)–(23), the atomic spin–orbit splitting is

$$E_{5/2}-E_{3/2}=\tfrac{5}{2}\zeta \quad \text{and} \quad \zeta=a_{3d}=\tfrac{2}{5}(E_{5/2}-E_{3/2}). \tag{24}$$

J. Chem. Phys., Vol. 115, No. 8, 22 August 2001

Hyperfine structure of Na₂   3651

A simple correspondence between molecular spin–orbit interaction constant and atomic spin–orbit interaction can be estimated below.

For $1\,^3\Delta_{3g}$ $(\Omega=3)$, the wave function is

$$|^3\Delta_{3g}\rangle=|\Lambda=2,\ \Sigma=1,\ \Omega=3\rangle=|\sigma_g\alpha\delta_g\alpha\rangle. \tag{25}$$

The diagonal matrix element of the spin–orbit term is

$$\langle\Lambda,\Sigma,S,\Omega,v|\mathbf{H}^{so}|\Lambda,\Sigma,S,\Omega,v\rangle=A_{\Lambda,v}\Lambda\Sigma. \tag{26}$$

So,

$$\langle^3\Delta_{3g}|\mathbf{H}^{so}|^3\Delta_{3g}\rangle=2A_{\Lambda,v}. \tag{27}$$

From the electron configuration of the $1\,^3\Delta_{3g}$ state, the spin–orbit interaction matrix element can also be written as

$$\langle^3\Delta_{3g}|\mathbf{H}^{so}|^3\Delta_{3g}\rangle=\sum_i\ \langle\sigma_g\alpha\delta_g\alpha|a\mathbf{l}_i\cdot\mathbf{s}_i|\sigma_g\alpha\delta_g\alpha\rangle$$

$$=\langle\delta_g\alpha|a\mathbf{l}\cdot\mathbf{s}|\delta_g\alpha\rangle. \tag{28}$$

Consider the admixture of $3d$ and $4d$ orbitals due to the necessity to minimize spatial overlap of the δ_g orbital with the valence $\sigma_g(ns)$ bonding orbital. The mixing of $4d$ into $3d$ is an overlap repulsion effect due to a charge distribution near the Na nucleus different from what it is on the free atom.

$$|\sigma_g 3s\rangle=N_{\sigma_g}(|3s\sigma_1\rangle+|3s\sigma_2\rangle), \tag{29}$$

$$1\equiv N_{\sigma_g}^2(1+2S+1), \tag{30}$$

where $S(R)=\langle3s\sigma_1|3s\sigma_2\rangle$ is a two center overlap which depends on internuclear distance. $N_{\sigma_g}=[2(1+S)]^{-1/2}$ is the normalization factor. $\sigma_g\delta_g$ corresponds to $[2(1+S)]^{-1}3s\,e^-$ on each Na atom. This is slightly less than 1/2 of a $3s\,e^-$, which shields (destabilizes) the $3d\delta\,e^{-1}$ from the Na$^+$ ion-core and also destabilizes the $3d\delta\,e^-$ by overlap repulsion. The $3d\delta$ orbital expands by mixing in some $4d\delta$ orbital character with the phase that reduces the electron density along the internuclear axis.

The admixture of $3d$ and $4d$ orbitals can be expressed as

$$|\delta_g\rangle=N(|\delta_g(3d)\rangle+\epsilon|\delta_g(4d)\rangle), \tag{31}$$

where $N=(1+\epsilon^2)^{-1/2}$ is the normalization factor and ϵ expresses the mixing of $4d$ into the nominal $3d$ orbital. If one substitutes Eq. (31) into Eq. (28), one obtains

$$\langle^3\Delta_{3g}|\mathbf{H}^{SO}|^3\Delta_{3g}\rangle=\langle\delta_g\alpha|a\mathbf{l}\cdot\mathbf{s}|\delta_g\alpha\rangle$$

$$=\frac{1}{1+\epsilon^2}[a(3d)+2\epsilon a(3d,4d)$$

$$+\epsilon^2 a(4d)]. \tag{32}$$
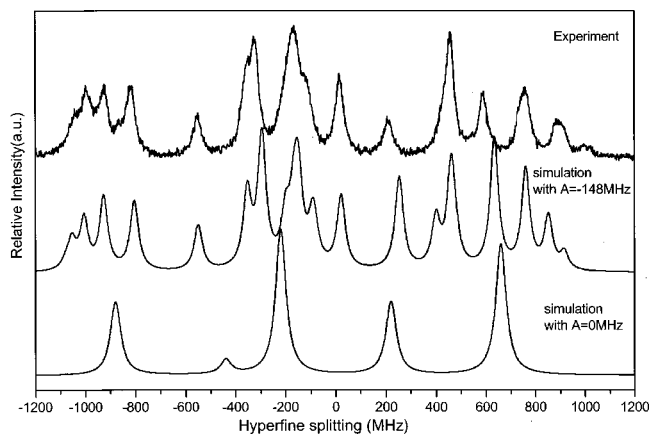
There is a relation for $a(nd)$[42]
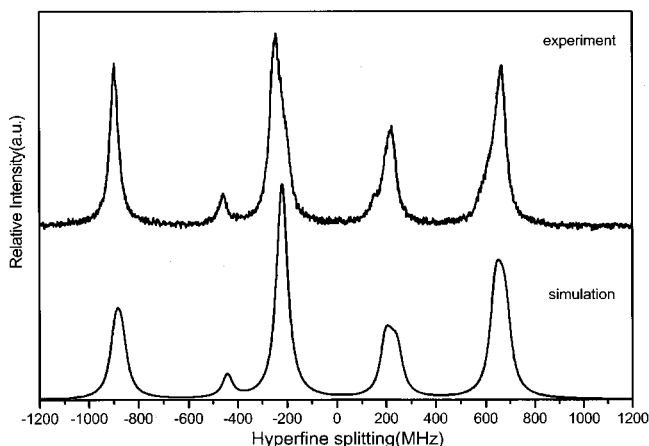
$$a(nd)\propto\frac{1}{n^3(l+1)(l+1/2)l}, \tag{33}$$

so

$$a(4d)=a(3d)(\tfrac{3}{4})^3=0.422a(3d) \tag{34}$$

and

(a)

(b)

FIG. 1. Experimental and calculated spectra with (a) $b_F=220$ MHz, $A=-148$ MHz, and $A=0$ MHz for $1\,^3\Delta_g$ $(v=14,\ N=2)\leftarrow b\,^3\Pi_{1u}$ $(v=25,\ J=2)$, and (b) with $b_F=220$ MHz, $A=-148$ MHz for $1\,^3\Delta_g$ $(v=17,\ N=22)\leftarrow b\,^3\Pi_{1u}$ $(v=28,\ N=22)$. All other constants are set to zero.

$$a(3d,4d)=[a(3d)a(4d)]^{1/2}=0.650a(3d). \tag{35}$$

From Eqs. (34) and (35), Eq. (32) becomes

$$\langle^3\Delta_{3g}|\mathbf{H}^{SO}|^3\Delta_{3g}\rangle=\left(\frac{1}{1+\epsilon^2}\right)a(3d)[1+2\epsilon(0.650)$$

$$+\epsilon^2(0.422)]. \tag{36}$$

From Eqs. (27) and (36), we obtain the relationship between the molecular spin–orbit interaction constant and the atomic spin–orbit interaction constant

$$A_{\Lambda,v}=\frac{1}{2}\left(\frac{1}{1+\epsilon^2}\right)a(3d)[1+2\epsilon(0.650)+\epsilon^2(0.422)] \tag{37}$$

$\epsilon<0$ is the right sign to cancel electron density near the bond axis. From the fit of the hyperfine spectra, the spin–orbit constant for the Na$_2$ $1\,^3\Delta_g$ state is very close to one tenth of the atomic Na $3d$ spin–orbit splitting, -148 MHz, and ϵ can be estimated to be -0.37.

Figure 1 gives a comparison between the observed OODR excitation spectrum and the calculated spectrum including only the Fermi-contact and spin–orbit interactions.
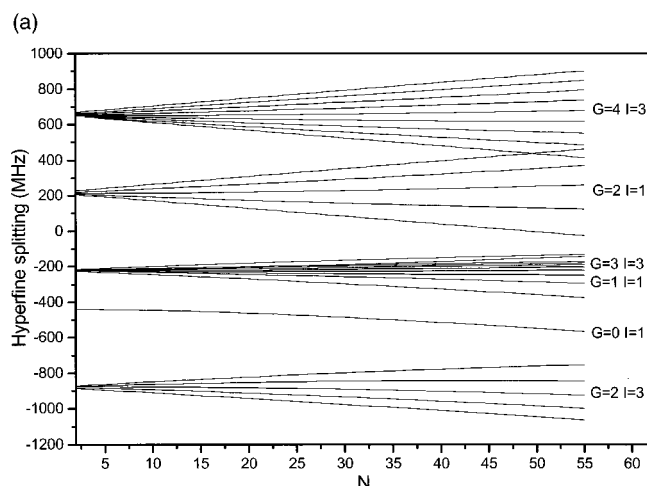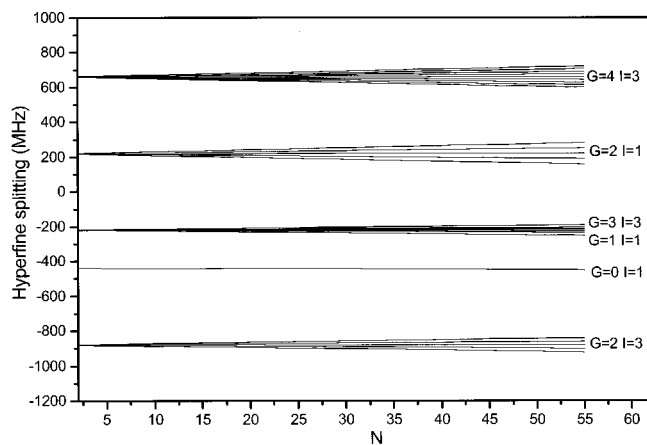
FIG. 2. Hyperfine splittings of the $1\,^3\Delta_g$ state calculated vs the rotational quantum number N with $b_F = 220$ MHz and (a) $\gamma = 0.005b_F$, and (b) $\gamma = 0.02b_F$.

FIG. 3. Hyperfine splittings in the $1\,^3\Delta_g$ state with $b_F = 220$ MHz, and (a) $\lambda = 50$ MHz, and (b) $\lambda = 150$ MHz.

In the calculation we take $b_F = 220$ MHz, a spin–orbit constant of -148 MHz, and all other interactions ($\mathbf{H}^{ss}, \mathbf{H}^{sr}$, etc.) are taken as zero. It is evident that the extra splitting of the low-N levels beyond what is observed at higher-N is mainly due to the diagonal spin–orbit term.

C. Spin–rotation interaction

There are three limiting hyperfine coupling schemes in case b: $b_{\beta N}$, $b_{\beta S}$, and $b_{\beta J}$. The $b_{\beta N}$ coupling case, nuclear spin $\mathbf{I}$ is first coupled to $\mathbf{N}$ to form an intermediate angular momentum $\mathbf{F}_1$, which then couples to spin $\mathbf{S}$ to generate the quantum number $\mathbf{F}$. Case $b_{\beta N}$ is seldom observed, because the much larger magnetic moment associated with the electron spin should couple much more strongly to $\mathbf{N}$ than does the nuclear magnetic moment. Cases $b_{\beta S}$ and $b_{\beta J}$ are the two usually observed hyperfine coupling cases in case b. Whether a state belongs (or is close) to cases $b_{\beta S}$ or $b_{\beta J}$ depends on whether the electron spin $\mathbf{S}$ interacts more strongly with the nuclear spin $\mathbf{I}$ (via Fermi-contact, $b_F\mathbf{I}\cdot\mathbf{S}$) or the rotational quantum number $\mathbf{N}$ (via spin–rotation, $\gamma\mathbf{N}\cdot\mathbf{S}$). If the spin–rotation interaction is stronger than the Fermi-contact interaction, the coupling order is that $\mathbf{S}$ is first coupled to $\mathbf{N}$ to
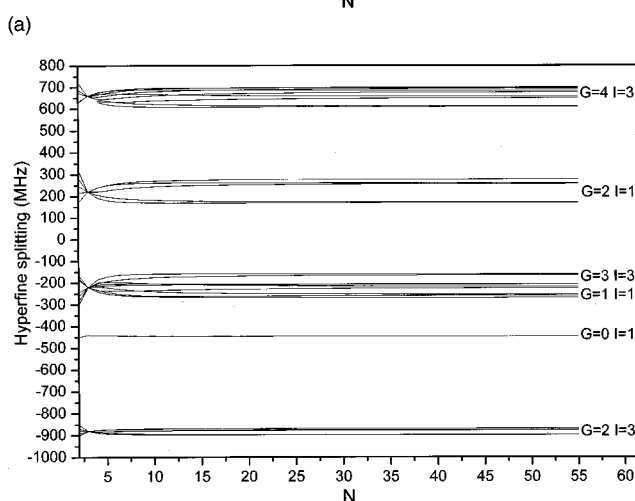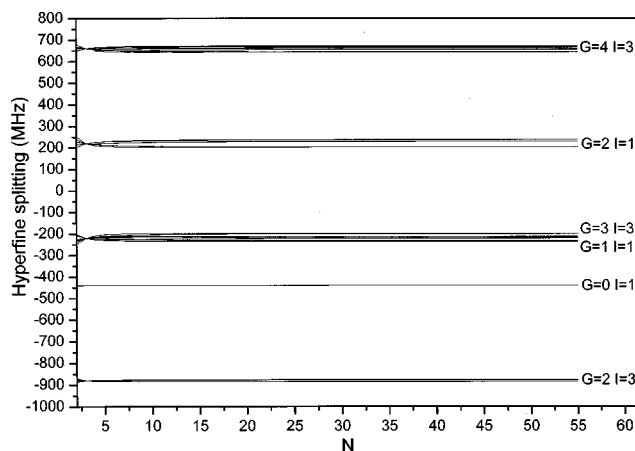
generate the intermediate angular momentum $\mathbf{J}$, which is then coupled to the nuclear spin $\mathbf{I}$ to form the total quantum number $\mathbf{F}$.

$$\mathbf{N}+\mathbf{S}=\mathbf{J}, \quad \mathbf{J}+\mathbf{I}=\mathbf{F}.$$

This coupling case is called case $b_{\beta J}$. In order for the Fermi-contact interaction to be extremely strong, an unpaired electron in a molecular orbital must have significant atomic s orbital character in order to have high-electron density at the nucleus as required by Eq. (9). In this case, electron spin $\mathbf{S}$ is first coupled to nuclear spin $\mathbf{I}$ to form the intermediate quantum number $\mathbf{G}$ which is then coupled to the rotational quantum number $\mathbf{N}$ to obtain the final quantum number $\mathbf{F}$.

$$\mathbf{S}+\mathbf{I}=\mathbf{G}, \quad \mathbf{N}+\mathbf{G}=\mathbf{F}.$$

This is called case $b_{\beta S}$.[31,43] As the rotational quantum number increases, the spin–rotation interaction inevitably becomes stronger, $\propto N$, and the coupling scheme will evolve from case $b_{\beta S}$ toward case $b_{\beta J}$.

That the coupling scheme of the Na$_2$1 $^3\Delta_g$ state is very close to case $b_{\beta S}$ for rotational levels up to $N=51$ indicates that the spin–rotation interaction remains negligible relative to the Fermi-contact interaction even for $N=51$ rotational levels. Figure 2 displays the calculated hyperfine splittings

J. Chem. Phys., Vol. 115, No. 8, 22 August 2001

Hyperfine structure of Na₂   3653

TABLE I. Relative line intensities for the transitions between the $1\,^3\Delta_g$ ($v=14$, $N=2$) and the $b\,^3\Pi_{1u}$ ($v'=25$, $J'=2$) states.

	$G=$	$F=$	$\Delta F=-1$	$\Delta F=0$	$\Delta F=+1$
		2	0.309	0	0.048
		3	0.691	0.117	0.102
	$G=4$	4	0.673	0.528	0.054
		5		1	0.027
		6			1
		1	1	0.044	
		2	1	0.056	0.048
$I=3$	$G=3$	3	0.382	0.2	0.014
		4	0	0.078	0.347
		5		0.222	0.98
		0	0.2		
		1	0.018	0.206	
	$G=2$	2	0.055	0.128	0.3
		3	0.273	0.011	0.571
		4	0.255	0.056	0.497
		0	0		
		1	0.073	0.067	
	$G=2$	2	0.2	0.311	0.014
		3		0.711	0.014
$I=1$		4			0.694
		1	0.218	0.206	
	$G=1$	2	0.036	0.117	0.082
		3		0.106	0.585
	$G=0$	2	0.073	0.05	0.34

for different values of the spin-rotation constant ($\gamma = 0.005b_F$, $0.02b_F$, and $b_F=220$ MHz) as the rotational quantum number N increases. As discussed above, the splittings of the low-N levels are dominated by the spin–orbit interaction. The calculation shows that the spin–rotation interaction constant, γ, must be smaller than $0.005b_F=1.1$ MHz in order to explain the high-N experimental results. Because the spin–rotation interaction constant is so small, we ignore this spin–rotation interaction term in our theoretical analysis. Previous studies show that the transition from $b_{\beta S}$ to $b_{\beta J}$ for the $2\,^3\Sigma_g^+$, $3\,^3\Sigma_g^+$, and $4\,^3\Sigma_g^+$ states of Na₂ occurs at much smaller N levels, implying that the spin–

rotation interaction is stronger in these states than in the $1\,^3\Delta_g$ states. This is because there is significant p character in all of these states, even the nominally $d\sigma$ states, and there can be no p character in $1\,^3\Delta_g$. Spin–rotation interaction is second order in $\mathbf{H}^{so}\otimes\mathbf{H}^{rot}$ and $\mathbf{H}^{so}$ is very small for d.

D. Spin–spin, spin–electronic, and rotation–electronic

Spin–electronic ($\mathbf{J}^\pm\cdot\mathbf{S}^\mp$) and rotation–electronic ($\mathbf{N}\cdot\mathbf{L}$) interactions have little effect on the hyperfine splittings of the $1\,^3\Delta_g$ state and are not considered in the hyperfine analysis. The spin–spin interaction term, λ, is usually smaller than second-order spin–orbit effects. The above spin–rotation analysis shows that spin–rotation is very small. This is conclusive evidence that the $\mathbf{H}^{so}$ contributions in second-order are always negligible for Na $3d$. This means that the non-negligible spin–spin contribution comes from a true microscopic spin–spin mechanism. Figure 3 shows the calculated hyperfine splitting as a function of rotational quantum number N for different values of the spin–spin interaction constant, (a) $\lambda=50$ MHz, (b) $\lambda=150$ MHz all with $b_F=220$ MHz. The calculated splitting patterns show that spin–spin interaction controls the hyperfine splittings within each G component and, at large N-values, becomes independent of N. From a comparison of the calculated splittings in Fig. 3 to the experimental spectra, a reasonable initial trial value of the spin–spin interaction constant is between 50 and 100 MHz for the simulation of hyperfine spectra (intensities and splittings).

E. Simulation of hyperfine spectra

The Na₂ $1\,^3\Delta_g\leftarrow b\,^3\Pi_{1u}$ transition intensities can be well approximated by a model of transitions from a case $a_\beta\,^3\Pi_{1u}$ state to a case $b_{\beta S}\,^3\Delta_g$ state. The $b\,^3\Pi_{1u}$ intermediate levels ($J=2-10$) are very close to case a_β coupling. An expression for the line strengths of transitions between these two coupling cases has been given in Ref. 27.

$$\langle\Lambda';S,\Sigma';J',\Omega',I,F'||T^1(\mu)||\Lambda;N,(SI)G,F\rangle$$

$$=\sum_J (-1)^{N+S+I+F}\sqrt{(2J+1)(2G+1)}\begin{Bmatrix} N & S & J \\ I & F & G \end{Bmatrix}(-1)^{J'+I+F+1}\sqrt{(2F+1)(2F'+1)}\begin{Bmatrix} J' & F' & I \\ F & J & 1 \end{Bmatrix}$$

$$\times\sum_{\Sigma,\Omega}(-1)^{N-S+\Omega}\sqrt{2N+1}\begin{pmatrix} J & S & N \\ \Omega & -\Sigma & -\Lambda \end{pmatrix}\sum_q(-1)^{J'-\Omega'}\sqrt{(2J+1)(2J'+1)}\begin{pmatrix} J' & 1 & J \\ -\Omega' & q & \Omega \end{pmatrix}$$

$$\times\langle\Lambda';S,\Sigma'|T_q^1(\mu)|\Lambda;S,\Sigma\rangle. \tag{38}$$

For the Na₂ $1\,^3\Delta_g\leftarrow b\,^3\Pi_{1u}$ case it is expressed as

$$\langle 1;1,0;J',1,I,F'||T^1(\mu)||2;N,(1I)G,F\rangle$$

$$=\sum_J(-1)^{J+I-1}(2J+1)\sqrt{(2J'+1)(2G+1)(2F+1)(2F'+1)(2N+1)}\begin{Bmatrix} N & 1 & J \\ I & F & G \end{Bmatrix}\begin{Bmatrix} J' & F' & I \\ F & J & 1 \end{Bmatrix}$$

$$\times\left[\begin{pmatrix} J & 1 & N \\ 1 & 1 & -2 \end{pmatrix}\begin{pmatrix} J' & 1 & J \\ -1 & 0 & 1 \end{pmatrix}\mu_0-\begin{pmatrix} J & 1 & N \\ 2 & 0 & -2 \end{pmatrix}\begin{pmatrix} J' & 1 & J \\ -1 & -1 & 2 \end{pmatrix}\mu_{-1}\right], \tag{39}$$

TABLE II. Nonlinear least-squares fit results of molecular constants for the Na$_2$ 1 $^3\Delta_g$ state ($v=14$).

$B_v = 0.112\,777\,55$ (cm^{-1}) (Ref. 37)
$D_v = 0.439\,696\,9 \times 10^{-6}$ (cm^{-1}) (Ref. 37)
$A = -158 \pm 5$ (MHz)
$\gamma = 0$ (MHz)
$\lambda = 80 \pm 10$ (MHz)
$a = 5 \pm 1$ (MHz)
$b_F = 220 \pm 5$ (MHz)
$c = 3 \pm 1$ (MHz)

where

$$\mu_0 \equiv \langle ^3\Pi_{1u} | T_0^1(\mu) | ^3\Delta_{1g} \rangle \approx 0,$$

$$\mu_{-1} \equiv \langle ^3\Pi_{1u} | T_{-1}^1(\mu) | ^3\Delta_{2g} \rangle. \tag{40}$$

The selection rule for nuclear spin quantum number I is $\Delta I = 0$. The total wave function (including both nuclear spins and rotation) should be antisymmetric with respect to permutation of the two Na nuclei. All $A \sim b$ mixed levels have e-parity because all A levels have e-parity. The even-J', e-parity antisymmetric levels of the b $^3\Pi_u$ state can only combine with symmetric nuclear spin wave functions with $I=3, 1$, while odd-J', e-parity symmetric levels of the b $^3\Pi_u$ state can only combine with antisymmetric nuclear wave
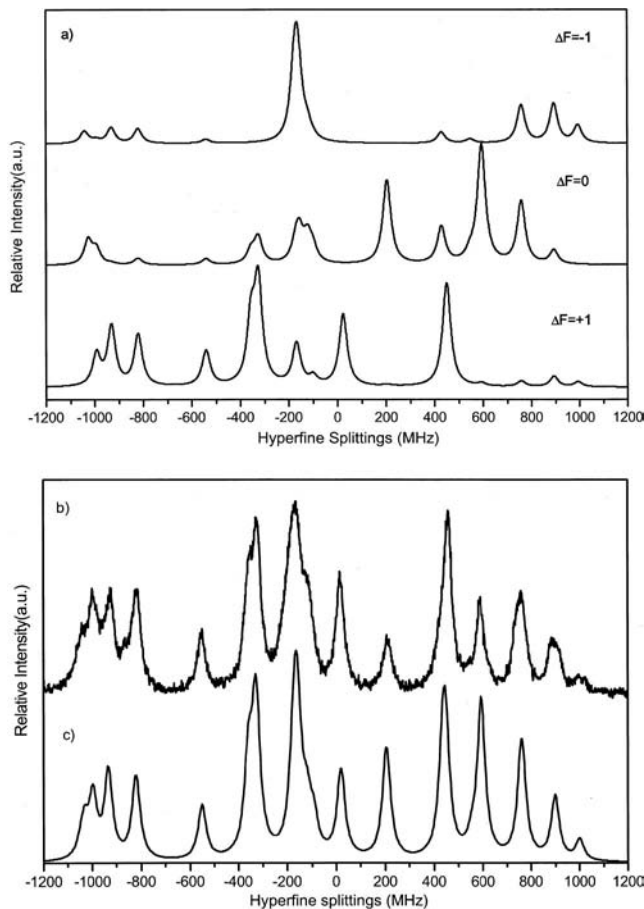

FIG. 4. (a) Theoretical simulation of hyperfine spectrum with the parameters listed in Table II for Na$_2$ 1 $^3\Delta_g$ ($v=14$, $N=2$)$\leftarrow b$ $^3\Pi_{1u}$ ($v=25$, $J=2$) for $\Delta F=-1$, $\Delta F=0$, and $\Delta F=+1$, respectively, (b) experimental spectrum and (c) summation of theoretical simulations in (a).
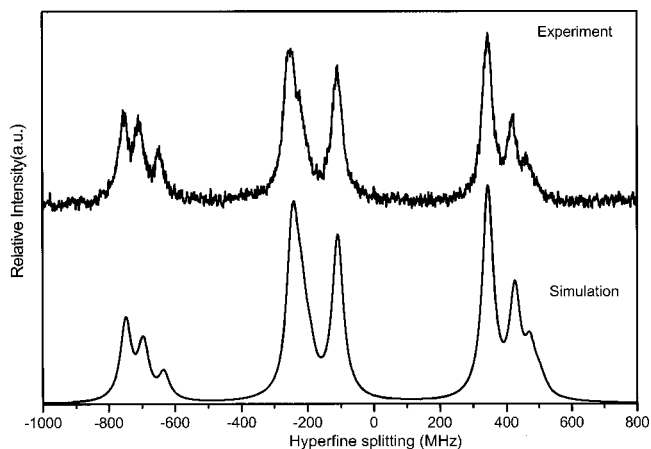

FIG. 5. (a) Experimental spectrum for transition 1 $^3\Delta_g$ ($v=14$, $N=5$)$\leftarrow b$ $^3\Pi_{1u}$ ($v=25$, $J=7$), and (b) theoretical simulation with parameters in Table II.

functions with $I=2, 0$. Thus, from even-J' levels of the b $^3\Pi_u$ state, we can reach nuclear-spin symmetric levels of the 1 $^3\Delta_g$ state with $I=3$, $G=4, 3, 2$, or $I=1$, $G=2, 1, 0$. Nuclear-spin antisymmetric levels with $I=2$, $G=3, 2, 1$, or $I=0$ $G=1$ can only be reached from odd-J' levels of the intermediate state. The transition selection rule for total quantum number F is $\Delta F=0,\pm 1$. As an example, the calculated relative transition intensities for 1 $^3\Delta_g$ ($v=14$, $N=2$)$\leftarrow b$ $^3\Pi_{1u}(J'=2,e)$ are listed in Table I. As the intermediate b $^3\Pi_{1u}$ state does not exhibit hyperfine splittings at 20 MHz resolution, the frequencies for all transitions to the same hypermultiplet component of the 1 $^3\Delta_g$ state are superimposed in the spectrum. The observed intensities are obtained by summing all possible transitions ($\Delta F=0,\pm 1$) to the same final F level.

F. Line shape simulation

Although the fine structure for the 1 $^3\Delta_g$ state was completely resolved, the hyperfine components were incompletely resolved for all rotational vibrational levels, It is difficult to determine the individual hyperfine frequencies by a
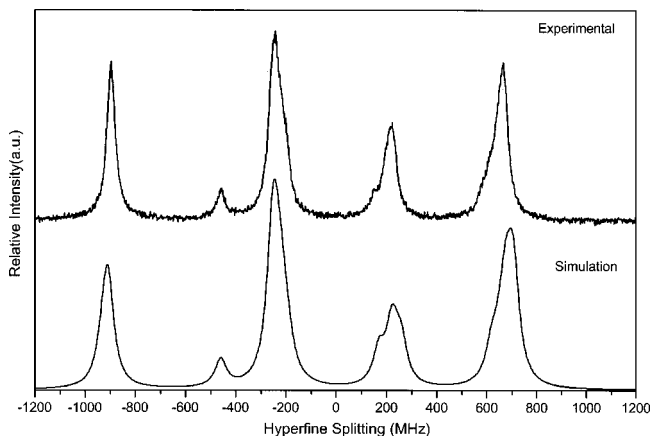

FIG. 6. (a) Experimental spectrum for transition 1 $^3\Delta_g$ ($v=14$, $N=22$)$\leftarrow b$ $^3\Pi_{1u}$ ($v=25$, $J=22$), and (b) theoretical simulation with parameters in Table II.
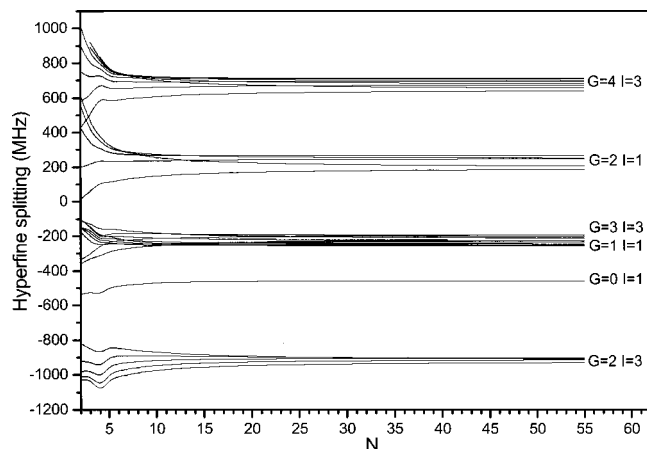
J. Chem. Phys., Vol. 115, No. 8, 22 August 2001

Hyperfine structure of Na$_2$

3655

FIG. 7. Hyperfine splittings of the Na$_2$ 1 $^3\Delta_g$ state vs the rotational quantum number N, calculated with parameters in Table II.

least-squares fit. The experimental hypermultiplet profiles are simulated as follows. The hyperfine energy levels for each rotational level are calculated by diagonalizing the full matrix described in Sec. III; the relative transition intensities can be calculated using Eq. (39). All transitions are assumed to have a Lorentzian shape with full width at half maximum (FWHM)=55 MHz,

$$I(\omega - \omega_0) = I_0 \frac{\gamma^2}{(\omega - \omega_0)^2 + (\gamma/2)^2}, \qquad (41)$$

where I_0 is the maximum at line center $\omega = \omega_0$ and FWHM $\delta\omega = \gamma$.

G. Nonlinear least-squares fit results and comparison with experimental spectra

Table II lists the results of the nonlinear least-squares fit of the molecular constants for the Na$_2$ 1 $^3\Delta_g$ state. Figure 4 shows the theoretical simulation for 1 $^3\Delta_g$ $v = 14$, $N = 2$ hyperfine spectra with $\Delta F = -1$, $\Delta F = 0$, $\Delta F = +1$ and the summation of all of these possible transitions and compares this simulation to the experimental spectrum. Figure 4 shows very good agreement between the experimental spectra and theoretical simulations. Figures 5 and 6 show comparisons between simulations and experiments with the same set of molecular constants for 1 $^3\Delta_g$ ($v = 14$, $N = 5$)$\leftarrow b$ $^3\Pi_{1u}$ ($v = 25$, $J = 7$) and 1 $^3\Delta_g$ ($v = 14$, $N = 22$)$\leftarrow b$ $^3\Pi_{1u}$ ($v = 25$, $J = 22$), respectively. Figure 7 shows the calculated hyperfine splittings of the 1 $^3\Delta_g$ state versus the rotational quantum number, N. The results show the evolution of the hyperfine splitting pattern as N increases, thus providing a global interpretation of the experimental spectra for *all* rotational quantum numbers N, both high-N and low-N.

V. CONCLUSIONS

We have expressed the hyperfine Hamiltonian for a homonuclear diatomic molecule in the Hund's case $b_{\beta S}$ basis. With this matrix, we theoretically calculated the hyperfine splittings for the Na$_2$ 1 $^3\Delta_g$ state. We reanalyzed the hyperfine spectra of Na$_2$ 1 $^3\Delta_g \leftarrow b$ $^3\Pi_{1u}$ transitions for both high- and low-rotational quantum numbers. With a nonlinear

least-squares fit, one set of optimized molecular constants is obtained. The molecular parameters thus determined result in good agreement between calculated and experimentally observed line profiles for rotational levels from $N = 2$ to the highest observed levels, $N = 51$.

Our analysis shows that the weak spin-orbit interaction of the 1 $^3\Delta_g$ state plays a major role for the hyperfine splittings of the low-N rotational levels. Effects of the electronic spin–rotation coupling ($\gamma \mathbf{N} \cdot \mathbf{S}$) to the HFS are negligible and do not play an important role for levels with $N \leqslant 51$. The separations between the G components depend on the Fermi-contact parameter, b_F. The electron spin–spin and nuclear spin–electron dipolar interactions give rise to the splittings within each group of G value and this splitting does not change with N as N increases up to $N \leqslant 51$.

We studied vibrational levels of $v = 13$–17. The HFS is not v-dependent within the vibrational levels we observed.

[1] I. C. Bowater, J. M. Brown, and A. Carrington, Proc. R. Soc. London, Ser. A **333**, 265 (1973).
[2] M. Broyer, J. Vigue, and J. C. Lehmann, J. Phys. (France) **39**, 591 (1978).
[3] T. A. Miller and R. S. Freund, J. Chem. Phys. **58**, 2345 (1973).
[4] M. D. Levenson and A. L. Schawlow, Phys. Rev. A **6**, 10 (1972).
[5] Y. Azuma, J. A. Barry, M. P. J. Lyne, A. J. Merer, J. O. Schroder, and J.-L. Femenias, J. Chem. Phys. **91**, 1 (1989).
[6] A. G. Adam and J. R. D. Peers, J. Mol. Spectrosc. **181**, 24 (1997).
[7] K. A. Walker and M. C. L. Gerry, Chem. Phys. Lett. **278**, 9 (1997).
[8] T. D. Varberg, R. W. Field, and A. J. Merer, J. Chem. Phys. **95**, 1563 (1991).
[9] B. Fernandez, O. Christiansen, P. Jorgensen, J. Byberg, J. Gauss, and K. Ruud, J. Chem. Phys. **106**, 1847 (1997).
[10] Li Li, Q. Zhu, and R. W. Field, J. Mol. Spectrosc. **134**, 50 (1989).
[11] J. B. Atkinson, J. Becker, and W. Demtröder, Chem. Phys. Lett. **87**, 128 (1982).
[12] Li Li, A. Yiannopoulou, K. Urbanski, A. M. Lyyra, B. Ji, W. C. Stwalley, and T. An, J. Chem. Phys. **105**, 6192 (1996).
[13] Li Li, A. Yiannopoulou, K. Urbanski, A. M. Lyyra, B. Ji, W. C. Stwalley, and T. An, J. Korean Phys. Soc. **32**, 309 (1998).
[14] Li Li, T. An, T.-J. Whang, A. M. Lyyra, W. C. Stwalley, R. W. Field, and R. A. Bernheim, J. Chem. Phys. **96**, 3342 (1992).
[15] Li Li and R. W. Field, J. Mol. Spectrosc. **123**, 237 (1987).
[16] Li Li, Q. Zhu, and R. W. Field, Mol. Phys. **66**, 685 (1989).
[17] G. Lazarov, A. M. Lyyra, Li Li, and J. Huennekens, J. Mol. Spectrosc. **196**, 259 (1999).
[18] C. Lisdat, H. Knockel, and E. Tiemann, J. Mol. Spectrosc. **199**, 81 (2000).
[19] A. Farbert and W. Demtroder, Chem. Phys. Lett. **264**, 225 (1997).
[20] H. Kato, M. Otani, and M. Baba, J. Chem. Phys. **91**, 5124 (1989).
[21] S. Kasahara, Y. Hasui, K. Otsuka, M. Baba, W. Demtroder, and H. Kato, J. Chem. Phys. **106**, 4869 (1997).
[22] R. Stringat, C. Athenour, and J. L. Femenias, Can. J. Chem. **50**, 395 (1972).

[23] T.-J. Whang, H. Wang, A. M. Lyyra, Li Li, and W. C. Stwalley, J. Mol. Spectrosc. **145**, 112 (1991).

[24] C. C. Tsai, J. T. Bahns, and W. C. Stwalley, Rev. Sci. Instrum. **63**, 5576 (1992).

[25] J. B. Atkinson, J. Becker, and W. Demtröder, Chem. Phys. Lett. **87**, 92 (1982).

[26] J. M. Brown, I. Kopp, C. Malmberg, and B. Rydh, Phys. Scr. **17**, 55 (1978).

[27] M. Barnes, A. J. Merer, and G. F. Metha, J. Chem. Phys. **103**, 8360 (1995).

[28] W. J. Balfour, A. J. Merer, H. Niki, B. Simard, and P. A. Hackett, J. Chem. Phys. **99**, 3288 (1993).

[29] A. G. Adam, Y. Azuma, J. A. Barry, A. J. Merer, U. Sassenberg, J. O. Schroder, G. Cheval, and J. L. Femenias, J. Chem. Phys. **100**, 6240 (1994).

[30] A. S.-C. Cheung, R. C. Hansen, and A. J. Merer, J. Mol. Spectrosc. **91**, 165 (1982).

[31] C. H. Townes and A. L. Schawlow, *Microwave Spectroscopy* (Dover, New York, 1975).

[32] Ian Mills *et al.*, *International Union of Pure and Applied Chemistry, Quantities, Units, and Symbols in Physical Chemistry*, 2nd ed. (Blackwell Scientific, Oxford, 1993).

[33] R. A. Frosch and H. M. Foley, Phys. Rev. **88**, 1337 (1952).

[34] W. Lichten, Phys. Rev. **120**, 848 (1960); A. N. Jette and P. Cahill, *ibid.*, **160**, 35 (1960).

[35] A. R. Edmonds, *Angular Momentum in Quantum Mechanics* (Princeton University Press, Princeton, NJ, 1960).

[36] R. N. Zare, *Angular Momentum: Understanding Spatial Aspects in Chemistry and Physics* (Wiley, New York, 1988).

[37] B. Ji, C.-C. Tsai, Li Li, T.-J. Whang, A. M. Lyyra, H. Wang, J. T. Bahns, W. C. Stwalley, and R. J. Le Roy, J. Chem. Phys. **103**, 7240 (1995).

[38] J. Li, Y. Liu, X. Dai, Li Li, and R. W. Field, J. Chem. Phys. **114**, 7859 (2001).

[39] J. Huennekens, I. Prodan, A. Marks, L. Sibbach, E. Galle, T. Morgus, and Li Li, J. Chem. Phys. **113**, 7384 (2000).

[40] C. E. Moore, Atomic Energy Levels, NSRDS Nat'l. Bur. Stand. No. 35 (U.S. GPO, Washington, D.C., 1971).

[41] H. Lefebvre-Brion and R. W. Field, *Perturbations in the Spectra of Diatomic Molecules* (Academic, San Diego, CA, 1986).

[42] E. U. Condon and G. H. Shortley, *The Theory of Atomic Spectra* (Cambridge University Press, Cambridge, 1979).

[43] T. M. Dunn, in *Molecular Spectroscopy: Modern Research*, edited by K. N. Rao and C. W. Mathews (Academic, New York, 1972).